Free Radical Biology and Medicine 115 (2018) 43–56

Contents lists available at ScienceDirect

Free Radical Biology and Medicine

journal homepage: www.elsevier.com/locate/freeradbiomed

Original article

Anti-tumor effects of cold atmospheric pressure plasma on vestibular schwannoma demonstrate its feasibility as an intra-operative adjuvant treatment

Yeo Jun Yoon[a], Michelle J. Suh[b], Hyun Young Lee[c], Hae June Lee[c], Eun Ha Choi[d], In Seok Moon[b,*], Kiwon Song[a,*]

[a] Department of Biochemistry, College of Life Science & Biotechnology, Yonsei University, Seoul 03722, Korea
[b] Department of Otorhinolaryngology, College of Medicine, Yonsei University, Seoul 03722, Korea
[c] Department of Electrical Engineering, Pusan National University, Pusan 46269, Korea
[d] Plasma Bioscience Research Center and Department of Electrical and Biological Physics, Kwangwoon University, Seoul 01897, Korea

ARTICLE INFO

Keywords:
Cold atmospheric pressure plasma (CAP)
Vestibular schwannoma (VS)
Adjuvant tumor treatment
Anti-tumor effect
Reactive oxygen species (ROS)
Necroptosis
Apoptosis

ABSTRACT

Vestibular schwannoma (VS), although a benign intracranial tumor, causes morbidities by brainstem compression. Since chemotherapy is not very effective in most *Nf2*-negative schwannomas, surgical removal or radiation therapy is required. However, depending on the size and site of the tumor, these approaches may cause loss of auditory or vestibular functions, and severely decrease the post-surgical wellbeing. Here, we examined the feasibility of cold atmospheric pressure plasma (CAP) as an intra-operative adjuvant treatment for VS after surgery. Cell death was efficiently induced in both human HEI-193 and mouse SC4 VS cell lines upon exposure to CAP for seven minutes. Interestingly, both apoptosis and necroptosis were simultaneously induced by CAP treatment, and cell death was not completely inhibited by pan-caspase and receptor-interacting serine/threonine-protein kinase 1 (RIK1) inhibitors. Upon CAP exposure, cell death phenotype was similarly observed in patient-derived primary VS cells and tumor mass. In addition, CAP exposure after the surgical removal of primary tumor efficiently inhibited tumor recurrence in SC4-grafted mouse models. Collectively, these results strongly suggest that CAP should be developed as an efficient adjuvant treatment for VS after surgery to eliminate the possible remnant tumor cells, and to minimize the surgical area in the brain for post-surgical wellbeing.

1. Introduction

Vestibular schwannoma (VS), although a benign intracranial tumor, can cause morbidities including hearing loss, tinnitus, dizziness, and possible mortality by brainstem compression [1,2]. The treatment strategies of VS are conservative, because both microsurgery and stereotactic radiation therapy pose risks of morbidity [3,4]. During the microsurgery of tumors with large volume, attempting the complete removal can increase the damage of cranial nerves, thereby leading to possible facial palsy or hearing loss. Minimizing the damage of cranial nerves during surgery may have a positive impact on the patient's wellbeing. On the other hand, incomplete resection can cause tumor recurrence [5,6]. Thus, a modified approach such as the subtotal removal followed by stereotactic radiosurgery is usually performed to prevent both neural damage complication and recurrence.

Unfortunately, there are several limitations of applying stereotactic radiosurgery to VS after surgery. Stereotactic radiosurgery has been reported to have risk of radiation hazard such as intracranial tumor swelling and to develop occasionally a new primary tumor in the intracranial region with the risk of radiation exposure [7–10]. Anti-cancer therapies such as chemo- and radio-therapy are based on the observation that malignant cancer cells tend to respond more sensitively to oxidative stress than normal cells [11–13]. However, unlike malignant cancer cells, benign tumors of the head and neck including VS express high levels of survivin, which enable tumor cells to be resistant to chemo- and radio-therapy [14–17]. Also, chemotherapy is not very effective in *Nf2*-negative schwannomas [18]. Thus, stereotactic radiosurgery to VS after surgery is not a preferred treatment approach and there is an increased need to develop an adjunct treatment for VS using new medical tools to overcome these obstacles. A novel adjunct therapy that efficiently removes the possible remnant tumor cells around cranial nerves would be helpful to minimize the surgical area to reduce the morbidity due to damage and the risk of recurrence.

Cold atmospheric pressure plasma (CAP) is an ionized gas generated

* Corresponding authors.
E-mail addresses: ISMOONMD@yuhs.ac (I.S. Moon), bc5012@yonsei.ac.kr (K. Song).

https://doi.org/10.1016/j.freeradbiomed.2017.11.011
Received 14 August 2017; Received in revised form 7 November 2017; Accepted 10 November 2017
Available online 11 November 2017
0891-5849/

by electrical discharges in the atmospheric pressure at room temperature (for a review, [19]). Currently, CAP has been extensively studied for clinical applications since it can be easily generated, causes no thermal damage to cells, and can be controlled by adding gases and/or adjusting the electric field (for a review, see [20]). CAP has been reported to induce cell death in various types of cancer cells *via* increasing the intracellular ROS (for a review, see [20]). However, CAP has been mostly applied to induce cell death in malignant tumors, and its effect on benign tumors has not yet been studied [21–25].

In this study, in order to verify the potential of CAP as an intraoperative adjunctive therapy of VS after surgery, we examined the effect of CAP on *Nf2*-deficienct human and mouse VS cell lines, primary VS cells, and tumor tissues derived from human patients. We also demonstrated the effect of CAP on recurrent tumor growth, when CAP was applied to the areas of surgical removal of a primary tumor in SC4-grafted mouse models.

2. Materials and methods

2.1. Air-based cold atmospheric generators for exposure of cell lines and mice

For cell exposure *in vitro,* CAP was generated by a micro dielectric barrier discharge (μ-DBD) plasma device (Fig. S1A), which is similar to the device reported by previously [26,27]. Air was used as the source of gas supply. The pump in the control device could pump out air to the CAP generator at 2 standard liters per minute (SLM) (Fig. S1B). Voltage and current were supplied by a circuit located inside the control device. The CAP-generating area covered an entire 35-mm culture dish (Fig. S1C). Optical emission spectroscopy (OES) confirmed that most of the radical species in the CAP generated by this device was nitrogen-based [27].

Fig. S1D and E show a planar-type CAP source for *in vivo* experiments of this study. This device was a surface dielectric barrier discharge (DBD)-type, which consisted of two copper electrodes covered on both sides of a dielectric plate. The dielectric plate was made of TLY-5A (Taconics, USA) material, which had a relative dielectric constant of 2.2 and a thickness of 0.254 mm. The copper electrodes on either side of the dielectric plate surface were of 2-μm thickness and the bottom electrode was patterned to generate plasma efficiently. The CAP source was attached to the bottom of the cover of a 35-mm culture dish, such that the plasma and the generated radical species remained inside the dish. The sinusoidal high voltage was applied to the copper electrodes located above with a peak-to-peak voltage of up to 8 kV at a driving frequency of 20 kHz, while the bottom electrode was grounded to prevent an electric shock to the cells. Plasmas were generated at the patterned surface of the electrode when the applied voltage was larger than the breakdown voltage, which was 5 kV in this system. The plasma density increased with an increase in applied voltage. The operation voltage was fixed as 6 kV for *in vivo* experiments, which was accompanied with 1.2 W discharge power of CAP. OES of CAP was recorded by USB2000+ (Ocean Optics, USA) in the wavelength range of 200–900 nm. The emission spectra of CAP generated from this device are shown in Fig. S1F. The major spectra included N_2 emission bands with a wavelength of 310–440 nm, and the N_2^+ emission bands from 391 to 428 nm. In addition to the nitrogen lines, several lines from oxygen were also generated.

pH of the cell culture medium after CAP treatment was measured using pH meter DELTA340 (Mettler Toledo, Columbus, OH, USA) (Fig. S1G). Ultraviolet radiation from this CAP source was measured by a UV meter (YK-37UVSD, Lutron Electronic Co., Taipei, Taiwan). Both CAP sources emitted UV-A and UV-C of less than 0.001 mW/cm2 (Fig. S1H, I). The ambient temperature was set to 20 ± 1.0 °C while the CAP was being processed into the cells or mice. The distance between the plasma source and the cells or mice was fixed at 8 mm.

2.2. Cell culture, CAP treatment, cell viability assay

Human VS HEI-193 cells were purchased from the American Type Culture Collection (ATCC; Manassas, VA, USA), and the *Nf*2-/- mouse Schwann (SC4) cells were obtained from the House Research Institute (HRI; Los Angeles, CA, USA). Both cells were cultured using Dulbecco's modified Eagle's medium (DMEM; Gibco-BRL/Invitrogen Corporation, Karlsruhe, Germany) supplemented with 10% fetal bovine serum (FBS; Sigma-Aldrich, St. Louis, MO, USA) and 1% penicillin/streptomycin (Gibco-BRL). Cells were maintained at 37 °C in a humidified atmosphere containing 5% CO_2.

HEI-193 and SC4 cells were cultured in 35-mm culture dishes. Twenty hours after seeding, cells were continuously exposed to CAP of 2 SLM for indicated time periods (1–10 min), and further incubated for a maximum of 72 h. Cell viability was monitored by spectrophotometric measurement of mitochondrial dehydrogenase activity using 3-(4,5-dimethylthiazol-2-yl)-2,5-diphenyl tetrazolium bromide (MTT; Sigma-Aldrich) [28]. The relative cell viability (%) of the CAP-treated cells was calculated by comparing its optical density at 570 nm with that of the untreated control cells.

2.3. Antibodies and reagents

Anti-PARP (1:1000), anti-p-RIPK1 (1:2000), anti-RIPK3 (1:1000), anti-Histone H3 (1:3000), and anti-β-actin (1:3000) (Cell Signaling Technology, Danvers, MA, USA), anti-phospho-Histone H2AX (1:2000, Merck Millipore, Temecula, CA), and anti-p-MLKL (1:2000, Abcam, Cambridge, MA, USA) antibodies were used with the indicated dilutions. Benzyloxycarbonyl-Val-Ala-Asp (OMe) fluoromethylketone (z-VAD(OMe)-fmk; z-VAD) and necrostatin-1 (Nec-1) were purchased from Cayman Chemical (Ann Arbor, MI, USA). N-Acetyl-L-cysteine (NAC; Sigma-Aldrich) was used as an anti-oxidant.

2.4. Immunofluorescence microscopy

HEI-193 and SC4 cells were seeded on the 35-mm culture dishes with coverslips, incubated for 20 h, exposed to CAP, and further incubated for indicated time periods. To examine the cellular propidium iodide (PI) uptake, coverslips were washed with warm phosphate buffered saline (PBS; Gibco-BRL), and incubated for 15 min with Hank's balanced salt solution (HBSS; Gibco-BRL) containing 10 μg/mL PI (Sigma-Aldrich) and 1 μM Hoechst 33342 (Sigma-Aldrich). Coverslips were washed twice with cold PBS and mounted with HBSS.

To detect the intracellular ROS, cells in the coverslips were washed with warm PBS and incubated with HBSS containing 5 μM 5(6)-carboxy-2′,7′-dichlorodihydrofluorescein diacetate (carboxy-H_2DCFDA; Invitrogen, Carlsbad, CA) for 30 min at 37 °C in the dark. Nuclei were co-stained with 1 μM Hoechst 33342. Coverslips were washed twice with cold PBS and mounted with HBSS. Images were collected using the Axio Imager A2 (Carl Zeiss, Jena, Germany) with AxioCam Hrc CCD camera (Carl Zeiss), and analyzed using the AxioVision software (Carl Zeiss).

2.5. Flow cytometry

Cells were detached and harvested at each time point using 0.25% trypsin–EDTA (Gibco-BRL), and washed with warm PBS. For PI uptake, cells were incubated with HBSS containing 10 μg/mL PI for 15 min. For Annexin A5–fluorescein isothiocyanate (Annexin V–FITC) and 7-Amino-Actinomycin (7-AAD) staining, cells were washed with binding buffer and incubated with PBS containing 1% Annexin V–FITC (BD Biosciences, NJ, USA) and 7-AAD (BD Biosciences) for 15 min according to the manufacturer's protocol. To measure mitochondrial superoxide, cells were incubated with warm HBSS containing 4.33 μM MitoSOX™ Red (Invitrogen) for 10 min in a CO_2 incubator at 37 °C. To determine the intracellular ROS level, cells were stained with 5 μM

carboxy-H_2DCFDA in HBSS for 30 min in a CO_2 incubator and washed twice with cold PBS. For cell cycle analysis, cells were fixed with 70% ethanol at −20 °C for 2 h, resuspended in 2% FBS, and were incubated with 100 μg/mL RNase A (Sigma-Aldrich) and 10 μg/mL PI for 15 min.

Flow cytometry was performed using BD FACSCalibur (BD Biosciences, CA, USA), analyzed with the BD CellQuest Pro software (BD Biosciences), and visualized using Flowing software 2.5.1 (www.uskonaskel.fi/flowingsoftware).

2.6. Determination of H_2O_2 concentration

The concentration of H_2O_2 was determined and the data was analyzed as described in Kurake et al. [29]. Phenol red lacking DMEM with 10% FBS was exposed to CAP in various spans and diluted 1:5 with 0.25 M sodium phosphate buffer. 50 μL of each was placed in individual wells of 96 well-plate and 50 μL of 100 μM Amplex® Red reagent (Invitrogen) with 0.2 U/mL horseradish peroxidase (HRP; Invitrogen) was added. Samples were incubated in the dark at room temperature for 30 min and the absorbance at 560 nm was measured according to manufacturer's protocol.

2.7. Western blotting

Cell lysates were prepared with the whole cell lysis buffer containing 2% SDS at pH 7.4. Samples of total proteins and histones were analyzed on an 8–15% gradient SDS–PAGE gel and electro-transferred to a PVDF membrane prior to the incubation with the primary antibody to detect the protein of interest. Western blotting was performed at least three times independently.

2.8. Human primary VS cells and sliced VS tissue preparation

All experiments based on the patients' cells and tissues were performed in accordance with the guidelines and were approved by the Severance Hospital Institutional Review Board (IRB No. 2016-2915-003). The primary VS cells were prepared from VS tumor tissues chopped with a surgical blade and digested using 0.25% Trypsin–EDTA (Gibco-BRL) for 10 min. The cells were cultured in a medium consisting of DMEM, 10% FBS, 1% penicillin/streptomycin, and 10% N2 supplement (Sigma-Aldrich). The VS tumor tissue slices were prepared from surgically removed tumors of 2-mm thickness and immersed in the medium containing DMEM, 10% FBS, 1% penicillin/streptomycin, and 10% N2 supplement.

2.9. SC4-grafted mouse model and CAP treatment procedure

All mouse experimental procedures were performed in strict accordance with the guidelines for the care and usage of laboratory animals by the Institutional Animal Care and Use Committee of the institute (IACUC), and were approved by the Animal Policy and Welfare Committee of Yonsei University College of Medicine (No. 2016-0055). A suspension of SC4 cells (8×10^5 or 2×10^5 cells/100 μL PBS) was injected subcutaneously into the flanks of fourteen (8×10^5 cells/100 μL PBS) and six (2×10^5 cells/100 μL PBS) 5-week-old female BALB/c nude mice (Central Lab Animal Inc., Seoul, Korea). Fourteen days after the injection, mice were anesthetized using a CO_2 chamber, and subcutaneous tumors were surgically removed. After the removal of tumors, one group of mice (n = 10) was treated with CAP for 10 min and the other group of mice (n = 10) were not treated with CAP to serve as controls. The lesions were then sutured and the mice in both the control and experimental groups were cultured. The volume (V) of the recurred tumor was measured at 10, 17, and 20 days after the tumor removal and CAP treatment with a caliper (Series 307, Asimeto Co., Germany). V in mm^3 was calculated using the equation (length x $width^2$)/2), where the length was based on the longest axis of the tumor. CAP-treated and -untreated mice were sacrificed after 10 days (n = 4 each); the remaining mice were sacrificed after 20 days (n = 3 each for 8×10^5 cells, n = 3 each for 2×10^5 cells), and the recurrent tumor from each mouse was removed. The weight of the resected tumor was measured with a GB204 balance (Mettler Toledo, Columbus, OH, USA)

2.10. Statistical analysis

All experiments were performed at least three times. Results are represented as the mean with standard deviation (SD). Statistical analysis was specified for each experiment using GraphPad Prism 6.01 (GraphPad Software Inc., CA, USA). Value of *$p < 0.05$, **$p < 0.01$, ***$p < 0.001$, and ****$p < 0.0001$ were considered statistically significant, and $p > 0.05$ was considered statistically not significant (ns).

3. Results

3.1. CAP shows highly efficient anti-proliferative effects in schwannoma cell lines

As the first step to validate the feasibility of CAP as an adjuvant treatment for VS after surgery, we examined the cellular effects of CAP exposure in both human HEI-193 and mouse SC4 VS cell lines that have been reported as *Nf2*-deficient [30,31]. We determined the optimal conditions of CAP treatment for anti-proliferative effects in HEI-193 and SC4 cells, by adjusting the exposure time and the volume of medium. HEI-193 and SC4 cells were exposed to single continuous air-based plasma of 2 SLM for 1–10 min and were further incubated for 3 days. The relative cell viability of the CAP-treated cells over the untreated control was determined every 24 h up to 72 h after the CAP treatment. A 7-min exposure to CAP had a sustained anti-proliferative effect on both HEI-193 and SC4 cells (Fig. 1A, B). With a 7-min CAP treatment, the relative cell viability of HEI-193 and SC4 cells further decreased as the volume of medium was reduced to 1 mL (Fig. 1C, D). Thus, CAP exposure of 7 min with 1 mL of medium was applied to HEI-193 and SC4 cells in the following experiments.

Next, we investigated whether the anti-proliferative effect of CAP on HEI-193 and SC4 cells entailed cell death by detecting propidium iodide (PI) uptake using fluorescence microscopy. Usually, PI does not penetrate intact cell membrane and its uptake is only observed in cells with membrane defects [32]. PI uptake was observed in HEI-193 and SC4 cells treated with CAP, while untreated cells showed no PI staining (Fig. 1E, F). This result was confirmed by measuring the PI uptake using flow cytometry. M2 peaks, which indicate the cell fractions with high PI uptake, increased in CAP-treated HEI-193 and SC4 cells (Fig. 1G, H). We also observed that the cell fractions in the M1 peaks (the intact cells) were shifted to M2 peaks upon increasing the incubation time from 24 h (black line) to 48 h (blue line) and 72 h (red line) (Fig. 1G, H). These results demonstrated that CAP has highly efficient anti-proliferative effect by inducing cell death.

3.2. ROS produced by CAP is majorly responsible for cell death in HEI-193 and SC4 cells

Previous studies have reported that CAP induces cell death in various types of malignant cancer cells *via* increasing the intracellular ROS [20]. Especially, ROS was reported as the main cause of cell death in human cervical cancer HeLa cells upon application of CAP generated by a similar device used in this study [26]. In order to examine whether the ROS produced by CAP induces cell death in non-malignant HEI-193 and SC4 cells, cells were pretreated for 2 h with 10 mM N-acetyl-cysteine (NAC), a general ROS scavenger, and exposed to CAP. Pretreatment of both HEI-193 and SC4 cells with an anti-oxidant NAC recovered the reduced viability by CAP exposure, compared to cells exposed to CAP alone, which showed a dramatic decrease in the relative cell viability (Fig. 2A, B).

Sustained excessive intracellular ROS are known to a hallmark of

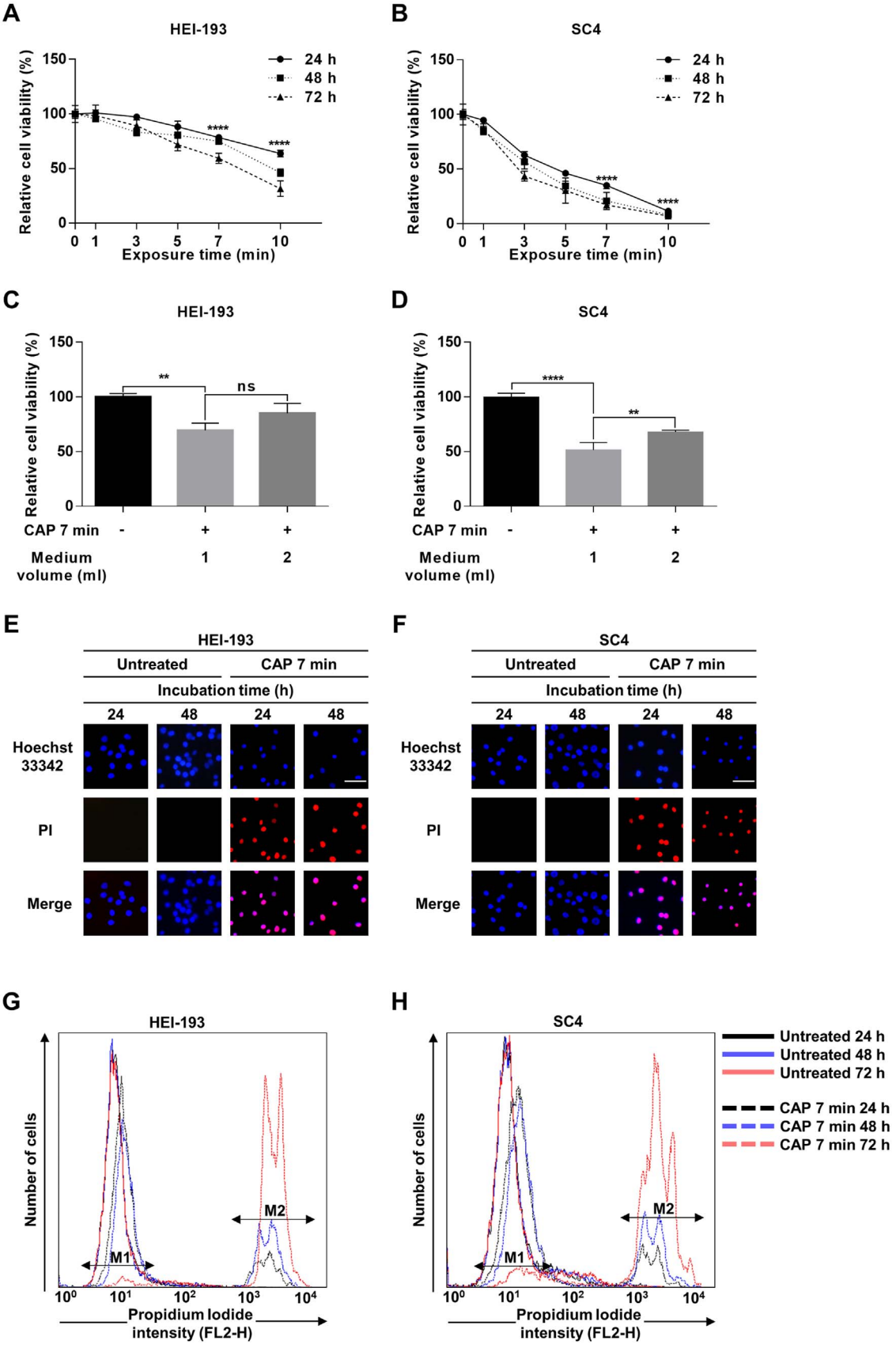

(caption on next page)

Fig. 1. *CAP efficiently induces cell death in HEI-193 and SC4 VS cells.* (A–H) HEI-193 and SC4 cells were treated with CAP for indicated exposure time and further incubated for 24, 48 (dotted line), and 72 (dashed line) h. (A, B) Relative cell viability was measured by the MTT assays. Result are shown as mean ± SD, n = 3. The p values shown in (A, B) were determined by two-way analysis of variance (ANOVA) with Bonferroni's post-hoc test. (C, D) HEI-193 and SC4 cells in different media volumes (1 mL and 2 mL) were treated with CAP for 7 min and further incubated for 18 h. Cell viability was measured by MTT assays. The relative viability over the untreated control was shown as mean ± SD, n = 3. The p values were determined by one-way ANOVA with Bonferroni's post-hoc test. The values of *p < 0.05, **p < 0.01, ***p < 0.001, and ****p < 0.0001 were considered statistically significant, and p > 0.05 was considered statistically not significant (ns). (E, F) Immunofluorescence microscopy images of PI uptake for cells treated with CAP for 7 min and further incubated up to 48 h. Nuclei were counter-stained with Hoechst 33342. Scale bar = 50 μm. (G, H) Flow cytometry results of PI uptake for HEI-193 and SC4 cells exposed to CAP for 7 min. CAP-treated cells were further incubated for 24 h (black line), 48 h (blue line) and 72 h (red line). For each flow cytometry analysis, 10,000 cells were counted and plotted.

cells undergoing apoptosis and necrosis [33], and are suggested as a main cause for cell death by CAP [34]. Thus, we also examined the intracellular ROS in HEI-193 and SC4 cells exposed to CAP with carboxy-H_2DCFDA. Although carboxy-H_2DCFDA is a non-fluorescent molecule, it is readily converted into a green-fluorescent form, when it is oxidized by intracellular ROS [35]. When HEI-193 and SC4 cells treated with CAP for 7 min were further incubated for 24 h and stained with 5 μM carboxy-H_2DCFDA, we observed a strong green fluorescence emitted by carboxy-H_2DCFDA in CAP-treated cells but not in the untreated control cells. These observations demonstrated that the ROS generated by CAP is mainly responsible for the anti-proliferative effect in HEI-193 and SC4 cells.

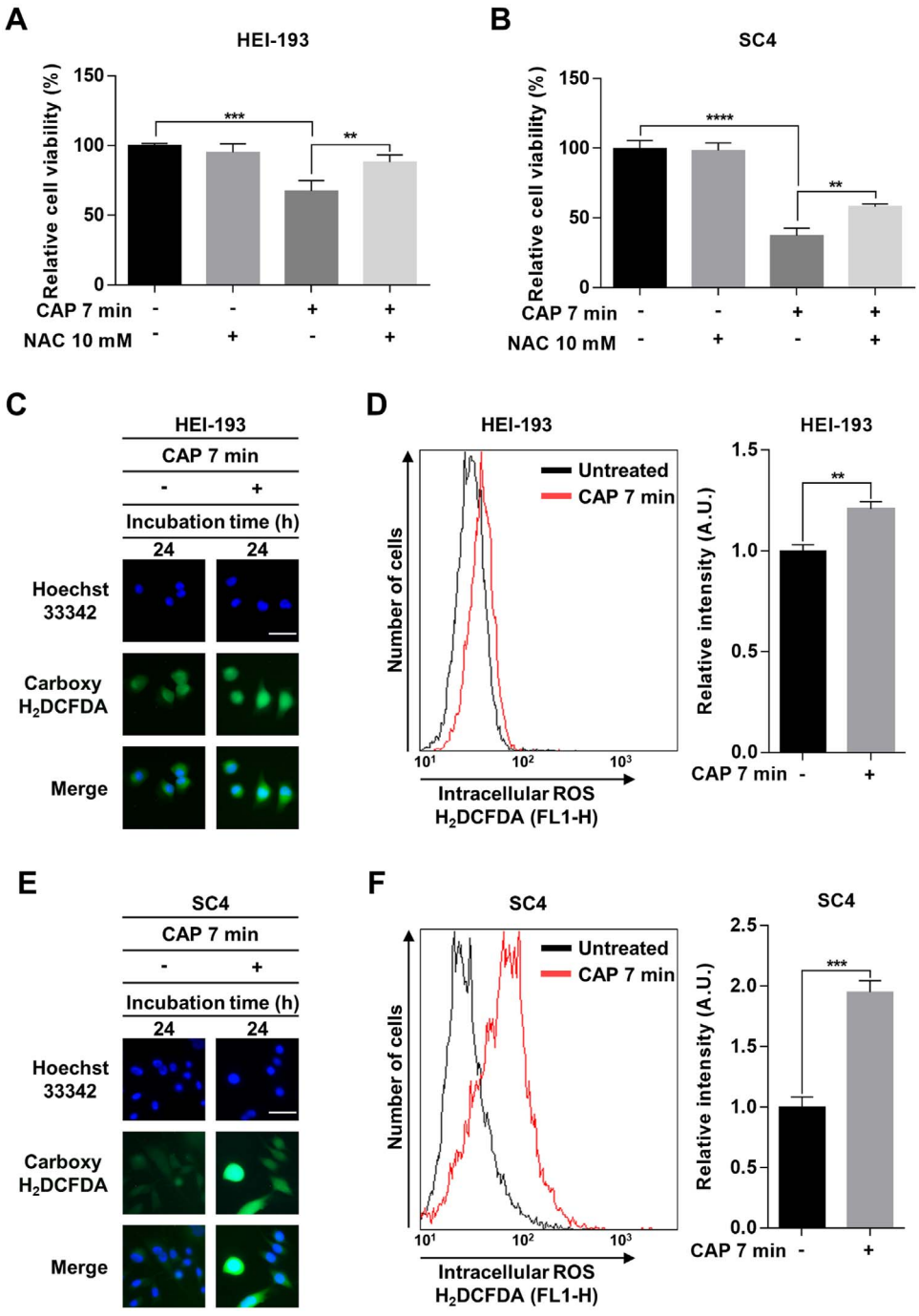

Fig. 2. *ROS is the main effector of CAP-induced cell death.* (A, B) HEI-193 and SC4 cells were exposed to CAP for 7 min in the presence or absence of 10 mM NAC, and further incubated for 18 h. Cell viability was measured by MTT assays and the relative cell viability over the CAP-untreated cells was plotted. Data are shown as mean ± SD, n = 3. The p values were calculated by one-way ANOVA with Bonferroni's post-hoc test. (C-F) HEI-193 and SC4 cells were exposed to CAP for 7 min, incubated for 24 h, and stained with 5 μM carboxy-H_2DCFDA. (C, E) Intracellular ROS were detected by fluorescent microscopy. Nuclei were stained with Hoechst. Scale bar = 50 μm. (D, F) Intracellular ROS in these cells were measured by flow cytometry. A representative plot was shown in the left panels, and the average of the relative fluorescence intensity of the CAP-treated over the untreated control, in three independent experiments, was presented in the right panels (geometric mean ± SD, n = 3). The p values were determined by unpaired *t*-test with Welch's correction. For each flow cytometric analysis, 10,000 cells were counted and plotted. The values of *p < 0.05, **p < 0.01, ***p < 0.001, and ****p < 0.0001 were considered statistically significant, and p > 0.05 was considered statistically not significant (ns).

Several studies have shown that hydrogen peroxide (H_2O_2) produced by CAP plays an important role in inducing cell death [29,36]. On the other hand, there are several reports that NAC functions as an anti-oxidant for various types of ROS, but cannot efficiently remove H_2O_2 at physiological pH [37]. As shown Fig. 2A and B, pre-treatment of NAC relieved the anti-proliferative effect of CAP, suggesting that hydrogen peroxide may not be a main cause of the CAP effect. In order to confirm whether the cell death by CAP in HEI-193 and SC4 cells was not mainly caused by H_2O_2, we directly treated HEI-193 and SC4 cells with the same concentration of H_2O_2 that is generated by CAP exposure. In order to do this experiment, we first measured the concentration of H_2O_2 in the media exposed to CAP with different spans from 1 to 10 min using an Amplex® Red reagent with HRP. The concentration of H_2O_2 in the CAP-treated media was increased in proportion to CAP exposure time (Fig. S2A). Next, we directly treated HEI-193 and SC4 cells with the same concentrations of H_2O_2 corresponding to different spans of CAP exposure for 24 h and measured the cell viability by MTT assay. Interestingly, cell viability did not decrease to a statistically significant level in H_2O_2-treated HEI-193 and SC4 cells (Fig. S2B). To confirm this result, we also treated HEI-193 and SC4 cells with twice higher concentrations of H_2O_2 than those of CAP-exposed media, but their cell viabilities were not significantly decreased (Fig. S2C). Collectively, these results suggest that H_2O_2 generated by CAP may not be a main cause for cell death by CAP and cell death by CAP might be a combinatorial effect of all reactive oxygen and nitrogen species produced by CAP.

3.3. CAP induces both apoptotic and necrotic cell death

To investigate the types of cell death induced by CAP, CAP-treated or untreated control HEI-193 and SC4 cells were stained with Annexin V/7-AAD and analyzed by flow cytometry. Phosphatidylserine (PS) is found only in the intracellular cell membranes of healthy cells, but during early apoptosis, it is bound by Annexin V upon translocating to the external cell membrane [38]. 7-AAD passes through cellular membranes, only when it becomes permeable or disrupted [39]. When cellular membranes break down during cell death, 7-AAD intercalates into the double-stranded DNA, which is mainly observed during late apoptosis and necrosis. Thus, cells that are 7-AAD-negative and Annexin V-positive are classified as early apoptotic cells. Late apoptotic cells are positive for both 7-AAD and Annexin V. Cells undergoing necrotic death are usually 7-AAD-positive and Annexin V-negative [39]. We observed 24.69% apoptotic and 43.80% necrotic cell distributions for HEI-193, and 48.40% apoptotic and 24.31% necrotic distributions for SC4 cells (Fig. 3A, B).

Because cell death by apoptosis and necrosis entails high concentration of superoxide in the mitochondria [40], we also measured the accumulation of mitochondrial superoxide in the CAP-treated HEI-193 and SC4 cells. We used MitoSOX™ Red that selectively labels only mitochondrial superoxide, followed by flow cytometry to determine the level of superoxide anion in mitochondria [40]. CAP treatment increased the mitochondrial superoxide levels by 2.23-fold in HEI-193 cells and by 2.37-fold in SC4 cells, when compared with that in the untreated cells (Fig. 3C). Collectively, these results demonstrated that CAP efficiently induces apoptotic and necrotic cell death in HEI-193 and SC4 cells.

3.4. CAP-induced cell death occurs in the presence of apoptotic and necroptotic inhibitors

As described, CAP-treated HEI-193 and SC4 cells underwent apoptosis and necrosis simultaneously. These cells have increased mitochondrial ROS that are also observed in the cells undergoing necroptosis [41]. Recent studies have classified necroptosis differently from necrosis (for a review, see [42]). Necroptosis, a programmed form of necrosis, is known to occur mainly through the ligand/cytokine of TNFR1, TRAIL-R or FAS, which belongs to the death receptor family, or by toll-like receptors and pathogens (for a review, see [43]). Physicochemical stresses have also been reported to induce necroptosis [44,45]. Because plasma exposure can be categorized under physicochemical stress, we investigated whether the necrotic cell death observed in the CAP-treated human HEI-193 cells was due to necroptosis.

Necroptotic signals activate RIPK1 by phosphorylation, and phosphorylated RIPK1 and receptor-interacting serine/threonine-protein kinase 3 (RIPK3) form necrosomes that bring about necroptosis by phosphorylating mixed lineage kinase domain like pseudo kinase (MLKL) [46,47]. However, RIPK3 has been reported to be silenced in many tumors (for a review, see [48]). In cells without RIPK3 expression, necroptosis does not occur because necrosomes cannot be formed; rather, RIPK1-dependent apoptosis is induced [49]. Thus, we first confirmed the expression of RIPK3 in HEI-193 cells under our experimental conditions as a prerequisite for necroptotic cell death, as shown in Fig. S3A. Next, in order to address the necroptotic cell death caused by CAP, we used pan-caspase inhibitor z-VAD-fmk (z-VAD) to block apoptosis and the RIP1 inhibitor Necrostatin-1 (Nec-1) to prevent necroptosis [50,51]. HEI-193 cells were pre-incubated with either z-VAD (10 μM), Nec-1 (20 μM) or both for 2 h, exposed to CAP, and further incubated for 18 h or 36 h to check the expression of key apoptotic and necroptotic markers: cleaved poly-(ADP-ribose) polymerase (PARP) for apoptotic cell death, and phosphorylated RIPK1 and MLKL for necroptosis. In the CAP-treated cells (lane 2), phosphorylated RIPK1 and MLKL as well as the cleaved PARP were clearly detected compared with that in the untreated control (Fig. 4A), demonstrating that both necroptosis and apoptosis are activated upon CAP exposure. When HEI-193 cells were pre-treated with z-VAD and exposed to CAP, the cleaved PARP was expressed at levels similar to that in untreated cells, and the increase in phosphorylated RIPK1 was similar to that seen in cells treated with CAP alone (lane 3, Fig. 4A). As expected, we observed that phosphorylated MLKL level was highly increased in z-VAD-treated cells, strongly supporting the activation of necroptosis by the block of apoptosis (lane 3, Fig. 4A). In the cells pretreated with Nec-1, the cleaved PARP was increased to levels similar to that in cells treated with CAP alone, while negligible levels of phosphorylated RIPK1 and MLKL were detected, comparable to that in the CAP-untreated control (lane 4, Fig. 4A). When HEI-193 cells were pre-treated with both z-VAD and Nec-1 and exposed to CAP, the expression of cleaved PARP and phosphorylated RIPK1 and MLKL was similar to that observed in CAP-untreated cells (lane 5, Fig. 4A). Altogether, these results demonstrated that CAP exposure induced necroptosis as well as apoptosis in HEI-193 cells.

Previous studies reported that z-VAD or Nec-1 alleviate DNA double-strand breaks (DNA–DSBs) and reduce the formation of γ-H2AX foci [52,53]. Because the above described experiments (Fig. 4A) showed that z-VAD and Nec-1 blocked the apoptotic and necroptotic cell death in CAP-treated cells, we hypothesized that z-VAD and Nec-1 also relieved DNA–DSBs in CAP-treated cells. Thus, we examined the DNA–DSBs in these cells by detecting the γ-H2AX levels. Surprisingly, DNA–DSBs were not decreased in the cells pre-treated with z-VAD or Nec-1, and rather increased in the cells pre-treated with both, compared with that in the cells treated with CAP alone (Fig. 4B). These observations strongly suggested that the effect of z-VAD and Nec-1 might be temporary, and necrosis occurred even when apoptosis and necroptosis were blocked.

Furthermore, when HEI-193 cells exposed to CAP in the presence of z-VAD and Nec-1 were incubated for 36 h, the cleaved PARP and phosphorylated RIPK1 and MLKL levels were significantly increased compared with that in CAP-untreated cells, regardless of the presence or absence of z-VAD and Nec-1 (Fig. S3B). These results also supported that z-VAD and Nec-1 only inhibit CAP-induced apoptosis and necroptosis temporarily.

To confirm the necrosis by CAP when apoptosis and necroptosis were blocked, we examined the relative cell viability in HEI-193 cells

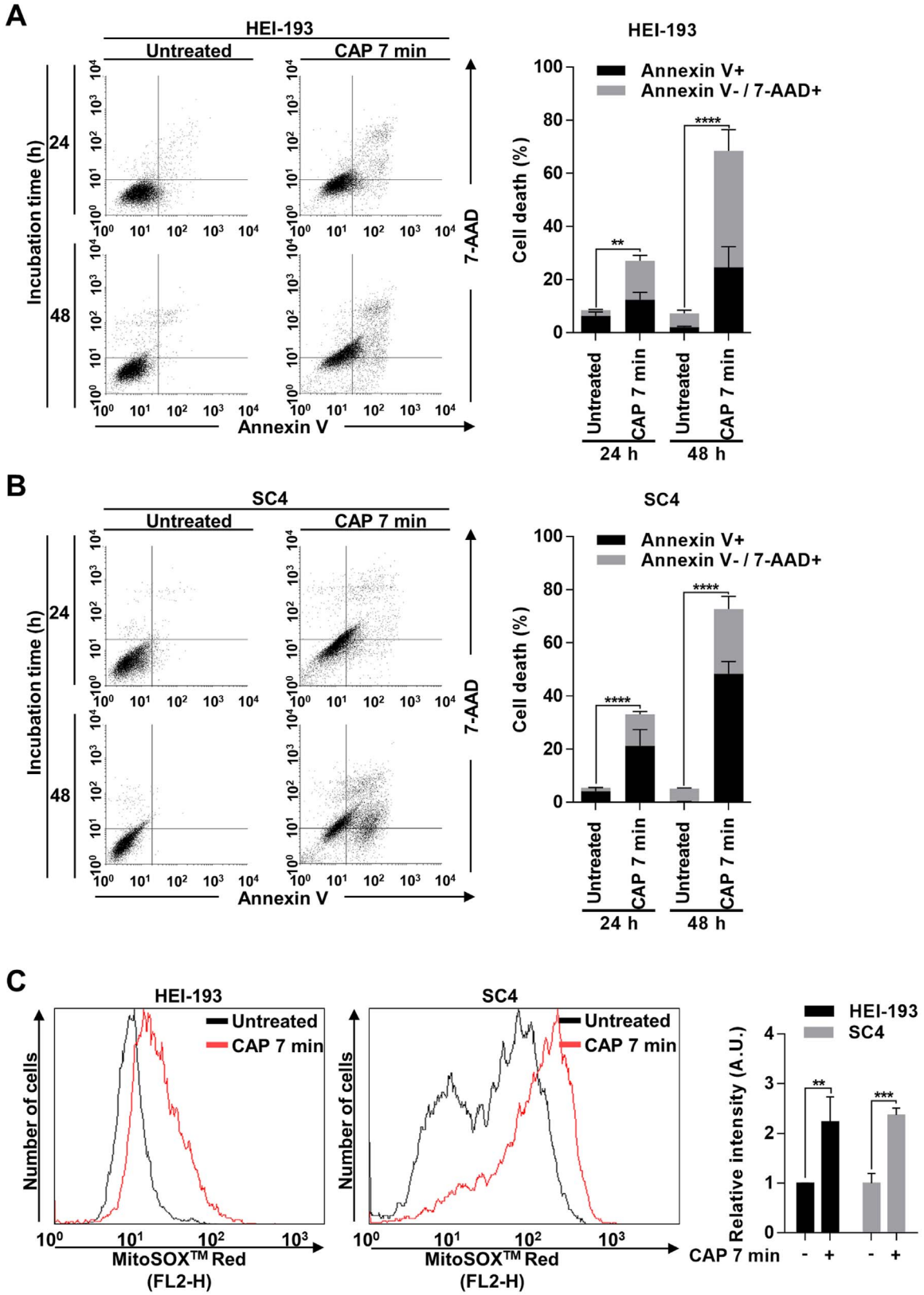

Fig. 3. *CAP induces necrotic as well as apoptotic cell death in VS cells.* (A, B) HEI-193 and SC4 cells were exposed to CAP for 7 min and further incubated for 24 and 48 h. These cells were analyzed by flow cytometry after 7-AAD and Annexin V–FITC staining. Each representative plot was shown in the left panel. From the quadrant plot of each experiment, the percent of cells in early apoptosis (bottom right of the quadrant), late apoptosis (top right), and necrosis (top left) were summed as dead cells. The average percent of dead cells from three independent experiments were plotted (mean ± SD, n = 3) in the right panels. (C) HEI-193 and SC4 cells were exposed to CAP for 7 min and further incubated for 24 h. In these cells, mitochondrial superoxide levels were measured by MitoSOX™ Red staining and flow cytometry. Representative histograms of data are shown in the left panels. The relative fluorescence intensity of the CAP-exposed cells over the untreated cells (1 A.U.) was calculated (A.U.; arbitrary unit), and the average of three independent experiments was plotted in the right panel (geometric mean ± SD, n = 3). For each flow cytometry analysis (A-C), 10,000 cells were counted. The p values shown in (A–C) were determined by two-way ANOVA with Bonferroni's post-hoc test. The values of *$p < 0.05$, **$p < 0.01$, ***$p < 0.001$, and ****$p < 0.0001$ were considered statistically significant, and $p > 0.05$ was considered statistically not significant (ns).

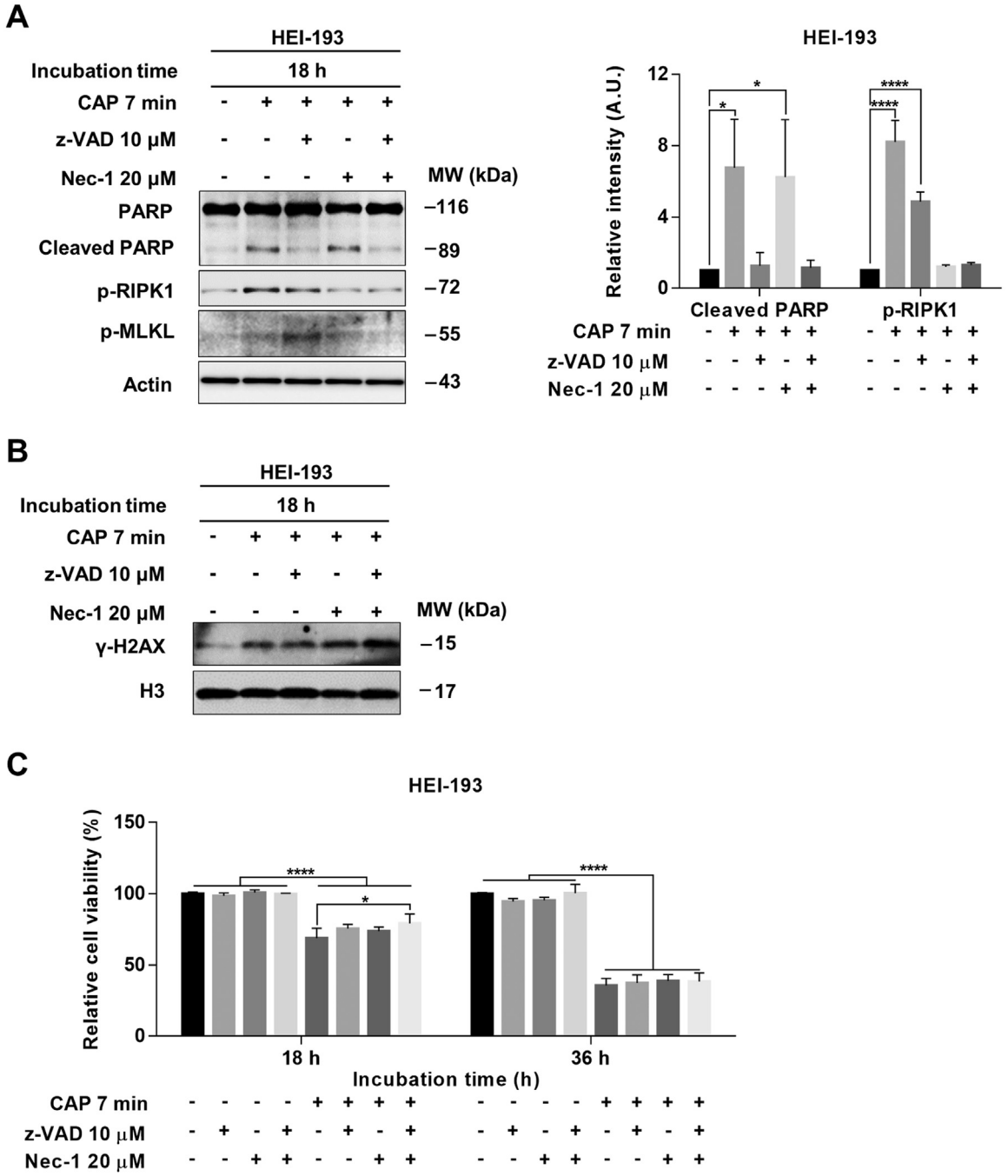

Fig. 4. *Cell death by CAP is not completely rescued by z-VAD-fmk and necrostatin-1.* (A, B) HEI-193 cells pre-treated with 10 μM z-VAD and/or 20 μM Nec-1 were exposed to CAP for 7 min and incubated for 18 h. The expression levels of cleaved PARP, p-RIPK1, RIPK3, p-MLKL, and γ-H2AX were detected by western blots. β-actin and histone H3 were used as loading controls. The relative band intensity of cleaved PARP and p-RIPK1 over β-actin from three independent experiments was plotted in the right panel as mean ± SD (n = 3 for each group). The p-values were determined by one-way ANOVA with Bonferroni's post-hoc test. (C) HEI-193 cells pre-treated with 10 μM z-VAD and/or 20 μM Nec-1 were exposed to CAP for 7 min and incubated for 18 and 36 h. Cell viability was measured by MTT assays and the relative cell viability of each sample over the untreated control from three independent experiments was presented as mean ± SD (n = 3 for each group). The p values were determined by two-way ANOVA with Bonferroni's post-hoc test. The values of *$p < 0.05$, **$p < 0.01$, ***$p < 0.001$, and ****$p < 0.0001$ were considered statistically significant, and $p > 0.05$ was considered statistically not significant (ns). Uncropped original western blots are shown in Fig. S4.

pre-incubated with z-VAD or Nec-1, or both. When these cells were examined at 18 h after CAP exposure, the relative viability of HEI-193 cells treated with both inhibitors (79.21%) was not at all recovered as that of untreated cells (Fig. 4C). When HEI-193 cells were examined at 36 h after CAP exposure, there were no significant differences in the relative cell viability between cells treated with CAP in the presence and absence of apoptotic and necroptotic inhibitors (Fig. 4C). Taken together, these results strongly suggested that CAP induces apoptosis, necroptosis, and necrosis, and when apoptosis and necroptosis were blocked by inhibitors, CAP-treated cells efficiently undergo cell death by necrosis.

3.5. CAP induces effective cell death in human primary VS cells and tumor tissues

So far, we showed that CAP effectively diminished the viability of

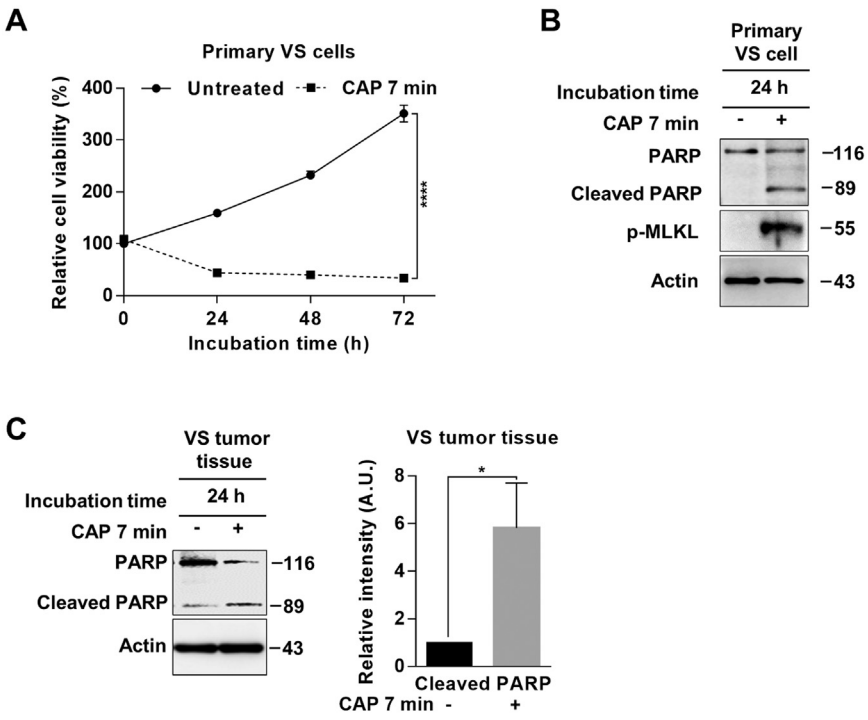

Fig. 5. *CAP induces apoptosis and necroptosis in human primary VS cells and VS tumor tissues.* (A, B) Human primary VS cells were treated with CAP for 7 min and further incubated for 24, 48, and 72 h. (A) Cell viability was measured through MTT assays from three independent experiments. The relative cell viability in each experiment was evaluated as a percentage relative to the viability of unexposed 0 h cells and was presented as mean ± SD (n = 3 for each group). The p values were determined by two-way ANOVA with Bonferroni's post-hoc test. (B) The expression levels of cleaved PARP and p-MLKL were detected in the 24 h-incubated samples by western blotting. β-actin was used as the loading control. (C) A patient-derived VS tumor mass was sliced into 2 mm thickness samples, treated with CAP for 7 min, and further incubated for 24 h to be homogenized. Expression of cleaved PARP was detected by western blotting. β-actin was used as the loading control. The average of the relative amount of cleaved PARP over β-actin from three independent experiments was plotted as mean ± SD (n = 3) in the right graph. The p values were calculated by unpaired *t*-test with Welch's correction. The values of $^{*}p < 0.05$, $^{**}p < 0.01$, $^{***}p < 0.001$, and $^{****}p < 0.0001$ were considered statistically significant, and $p > 0.05$ was considered statistically not significant (ns). Uncropped original western blots are shown in Fig. S4.

HEI-193 and SC4 cells. Because tumor cell lines often lose their original properties during long-term subculture [54], we examined the effect of CAP in primary VS cells from the patients. A CAP exposure for 7 min (the same exposure conditions as that for the human HEI-193 cell lines) effectively decreased the relative cell viability in primary VS cells (Fig. 5A). Comparison of the relative viabilities revealed that CAP seemed to be exert more effects on the primary cells than on HEI-193 cells (Figs. 1A and 5A). We further confirmed that the decreased relative viability by CAP in the primary VS cells was due to apoptosis and necroptosis by assessing the cleaved PARP and p-MLKL levels (Fig. 5A, B). Thus, we validated that the CAP treatment effectively induces cell death in primary VS tumor cells.

We also examined the effect of CAP in the patient-derived VS tumor tissues. Recent studies have shown that CAP penetrates up to 1.5 mm from the tissue surface [55,56]. Thus, we sectioned the primary tumor mass into slices of 2-mm thickness, exposed to CAP for 7 min, and examined the levels of cleaved PARP at 24 h after CAP exposure. The cleaved PARP was highly increased in the CAP-treated tissue samples (Fig. 5C). These results suggested that CAP efficiently induces cell death in the tumor tissues of at least 2-mm thickness, implying that CAP would be efficient as an adjuvant treatment for the remnant VS tumor cells in tissues after the main tumors were surgically removed.

3.6. CAP reduces the recurrent tumor growth after resection in SC4-grafted mouse

Recently, a study on the plasma-based tumor therapy reported that the promising outcomes from *in vitro* research are not reproducible in a mouse model [57]. Thus, we examined the anti-proliferative effect of CAP on VS *in vivo* using SC4-grafted BALB/c nude female mice, especially when applied after surgery to prevent or slow down the VS recurrence. A new air-based CAP device was designed to apply plasma on the operation wound of a mouse (Fig. S1D and E), and the anti-proliferative effect of CAP, generated from this device, was verified. When SC4 cells were treated with CAP from this device for different exposure times ranging from 1 to 10 min, and incubated for 24, 48, and 72 h, the relative cell viability was severely reduced at 5 min or longer exposures (Fig. 6A).

We also examined whether the decreased viability in SC4 cells was the effect of CAP, and not due to the ultraviolet rays (UV) or heat produced during the generation of CAP. To address this, the relative viability of SC4 cells exposed to direct CAP was compared with that of the cells exposed to CAP but whose culture medium was immediately exchanged to a fresh one (recovered group), after a 24-h incubation. Further, the relative viability was also examined in SC4 cells that were not directly exposed to the CAP but were incubated with the medium pre-exposed to plasma for 10 min (PAM; plasma-activated medium group) [58]. Viability of the recovered group was almost identical to that of the CAP-untreated cells, while the PAM group showed viability similar to that of the cells exposed to CAP for 10 min (Fig. 6B).

Because we used a new CAP device for mouse *in vivo* treatment, we also examined whether the cell death effect in SC4 cells by a new CAP device was cause by H_2O_2 produced by CAP. To answer this question, we first measured the concentration of H_2O_2 in the media exposed to CAP for 10 min, which led to complete cell death in 24 h as shown in Fig. 6A. Its H_2O_2 concentration was 133 μM. Next, we directly treated SC4 cells with the same concentration of H_2O_2 (133 μM) and incubated for 24 h. The cell viability of these cells did not decrease statistically significantly (Fig. 6C). These results demonstrated that the anti-proliferative effect observed upon the treatment of CAP produce by an *in vivo* device was due to CAP and its components, and not by UV, heat, or H_2O_2 alone.

With the new plasma device that could apply CAP to the mouse wound, we examined the anti-proliferative effect of CAP on VS after surgery, to prevent or slow down the VS recurrence. As described in Fig. 6D and E, fourteen BALB/c nude mice were injected with 8×10^5 SC4 cells on the flank, examined for tumor growth for 14 days, and the tumor was surgically ablated from each mouse as much as possible. The surface of the surgical wound area after tumor removal was irradiated with CAP for 10 min in seven mice (n = 7), while the other seven mice were incubated without any CAP exposure and served as controls (n = 7). The volume of recurred tumor in the CAP-treated and -untreated mice was measured at 10, 17, and 20 days after surgery. The recurrent tumor from each mouse was surgically removed at day 10 and 20, and its weight was examined. After surgery, we could observe regrowth of the tumor in both CAP-treated and -untreated mice, but the volume of

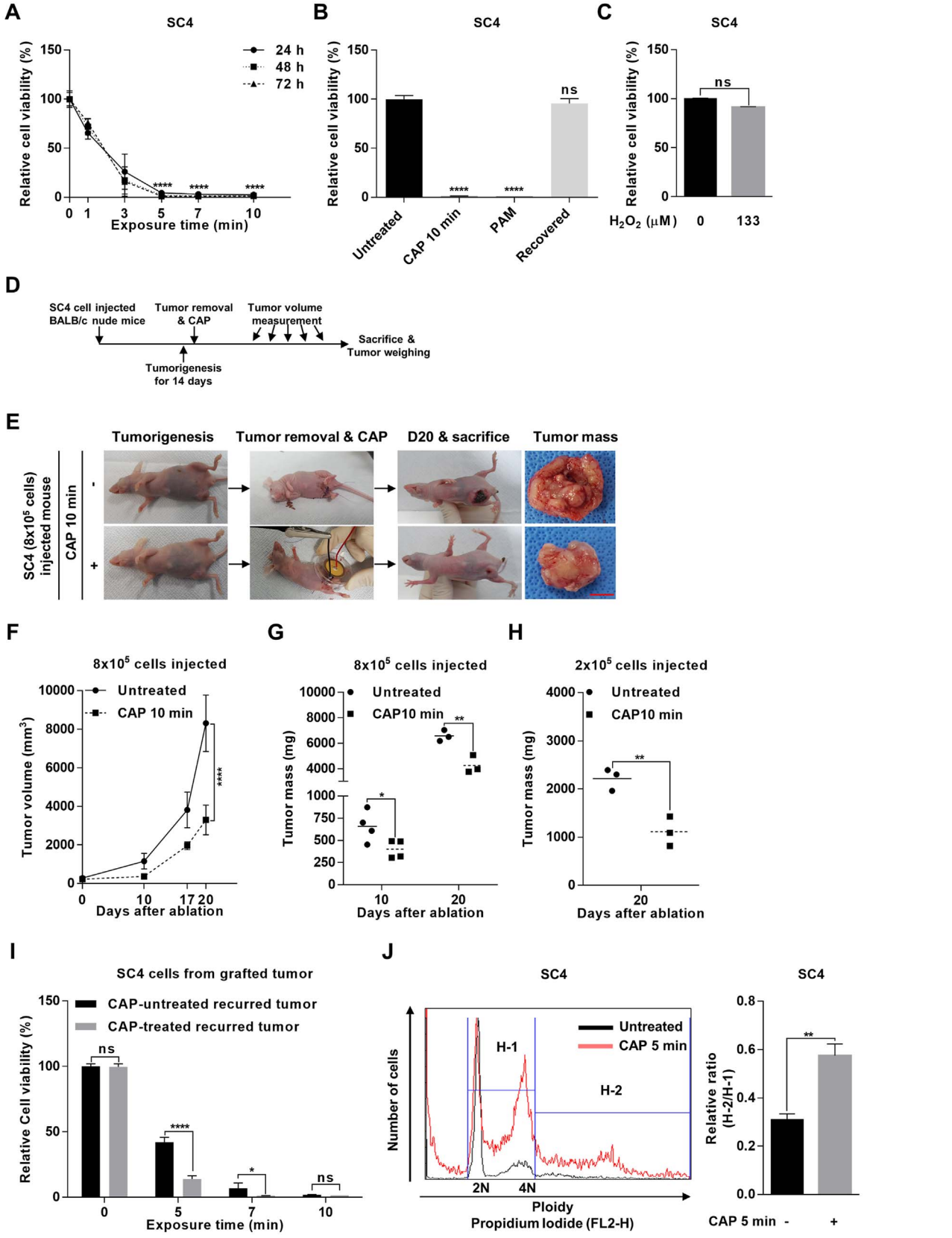

(caption on next page)

Fig. 6. *CAP treatment after the ablation of tumor reduces the recurrent tumor growth in SC4-grafted nude mice.* (A) SC4 cells were treated with CAP for indicated exposure times and further incubated for 24, 48, or 72 h. Cell viability was measured by MTT assays. The average of the relative viability of the CAP-treated over the untreated cells was plotted as mean ± SD, n = 3. The p values were determined by two-way ANOVA with Bonferroni's post-hoc test. (B) The viability was tested by MTT assays in the following samples after 24 h of incubation: SC4 cells treated with CAP for 10 min (CAP 10 min), SC4 cells treated with CAP for 10 min and its culture medium immediately replaced with the fresh culture medium (recovered), and SC4 cells whose original medium was replaced with the culture medium exposed to CAP for 10 min (plasma activated medium, PAM). The relative cell viability of these samples over the CAP-untreated control was plotted as mean ± SD, n = 3. The p values were determined by one-way ANOVA with Bonferroni's post-hoc test. (C) SC4 cells were treated with 133 μM H_2O_2, which corresponds to the concentration of H_2O_2 in the media exposed to CAP from a new device for 10 min, and incubated for 24 h. Cell viability was measured by MTT assays and the relative cell viability over the untreated cells was plotted. Data are shown as mean ± SD, n = 3. The p values were calculated by Mann-Whitney test. (D) A schematic diagram of the experimental procedures for CAP treatment of SC4 cell-grafted BALB/c nude mouse model of VS. (E–H) Tumors were removed from 8×10^5 or 2×10^5SC4 cell-grafted BALB/c nude mice by microsurgery and the surgery areas were either exposed to CAP for 10 min or left untreated to serve as controls. These processed mice were examined for 20 days after the surgery and CAP-treatment. (E) They were sacrificed at day 20 and the representative tumor mass at day 20 was shown, red bar = 1 cm. (F) During 20 days of incubation, tumor volume of each mouse was measured at days 10, 17, and 20, and the average tumor volume of the CAP-treated and the control mice was plotted as mean ± SD (n = 7 for day 10, n = 3 for day 17 and 20 each). The p values were determined by two-way ANOVA with Bonferroni's post-hoc test. (G) Tumor mass of each sacrificed mouse was weighed at day 10 and 20, and plotted as mean ± SD (n = 4 for day 10 and n = 3 for day 20). The p values were calculated by multiple *t*-test with Holm-Sidak method. (H) Tumors were removed from 2×10^5 SC4 cell-grafted BALB/c nude mice by microsurgery and the surgery areas were either exposed to CAP for 10 min or left untreated to serve as controls. These mice were sacrificed at day 20 and their tumors were removed. The weight of tumors was plotted as mean ± SD (n =3 for day 20). The p values were calculated by unpaired *t*-test with Welch's correction. (I) SC4 cells isolated from the recurred tumors of (E) and (G) were cultured and exposed to CAP for indicated time periods and further incubated for 24 h. Cell viability was determined by MTT assays, and the average of the relative cell viability over the CAP-untreated control was shown as mean ± SD (n = 3). The p values were determined by two-way ANOVA with Bonferroni's post-hoc test. (J) The ploidy of SC4 cells were determined by flow cytometry, after SC4 cells were exposed to the CAP from the *in vivo* device used for 5 min and incubated for 24 h. For each flow cytometric analysis, 10,000 cells were counted. Based on the ploidy by flow cytometry in the left panel, the proportion of aneuploid cells was determined by the ratio of cells with the abnormal ploidy range (H-2) over the cells with normal ploidy range (H-1). The average ratio of the aneuploidy from three independent experiments was plotted as mean ± SD (n = 3) in the right graph. The p values were calculated by unpaired *t*-test with Welch's correction. The values of *p < 0.05, **p < 0.01, ***p < 0.001, and ****p < 0.0001 were considered statistically significant, and p > 0.05 was considered statistically not significant (ns).

tumor in the CAP-untreated mice was on an average 3.16-fold and 2.52-fold bigger at day 10 and day 20, respectively (Fig. 6F). The relative weight of the extracted tumor of CAP-treated over -untreated was, on an average, 60.9% at day 10 and 66.7% at day 20 (Fig. 6G). In order to confirm the similar effect of CAP treatment when the tumor size is small, we injected 2×10^5 SC4 cells on the flank of six BALB/c nude mice and followed the same experimental procedures. The surface of the surgical wound area after tumor removal was irradiated with CAP for 10 min in three mice (n = 3), while the other three were incubated without any CAP exposure and served as controls (n = 3). At day 20 after the CAP treatment, all mice were sacrificed and their tumors were weighed after surgical removal. On average, the weight of the tumor from the CAP-treated mice was 50.2% smaller than that of the untreated mice (Fig. 6H). These results strongly demonstrated that CAP was effective in slowing down the growth of the recurrent tumor, suggesting CAP exposure as a promising adjuvant treatment for VS after surgery.

Because some studies have shown that tumor cells survived from therapies can gain resistance to the therapies applied [59,60], we also investigated whether the VS cells from the recurrent tumor after CAP-treatment became resistant to the anti-proliferative effect of CAP. We cultured the SC4 cells extracted from the recurrent tumors from the CAP-treated and -untreated SC4-grafted nude mice (Fig. 6E) and compared the relative cell viability, after being exposed to CAP for 5, 7, and 10 min and further incubated for 24 h. The relative cell viability was efficiently decreased in the SC4 cells obtained from the CAP-exposed tumors. These cells were even more sensitive to the induced cell death caused by CAP exposure than the cells from the CAP-untreated tumors (Fig. 6I).

Why then would the SC4 cells obtained from the CAP-exposed recurrent tumors be more sensitive to CAP treatment than the SC4 cells from the CAP-untreated recurrent tumors? Several studies have reported that DNA damage by oxidative stress leads to aneuploidy, which attenuates proliferative capacity of cells and induces cell death [61,62]. We, thus, examined whether the cells with aneuploidy increased upon CAP treatment. SC4 cells exposed to CAP for 5 min and incubated for 24 h were stained with PI and sorted by ploidy using flow cytometry. CAP-treated SC4 cells showed a 1.85-fold higher aneuploidy ratio compared with the unexposed control cells (Fig. 6J). These results suggested that DNA damage by CAP treatment induces aneuploidy, which makes CAP-treated cells become more susceptible to cell death by the subsequent CAP treatment.

4. Discussion

Vestibular schwannoma (VS) is an intracranial benign tumor, and sometimes needs to be surgically removed because of its possible risk of brain stem compression [1,2]. However, its complete removal without cranial nerve damage is difficult, particularly in the case of a huge tumor [63]. In addition, most VSs with *Nf*2 deletion do not respond well to conventional chemotherapy [18], and may arise at multiple sites, making radiotherapy less successful [18,64]. Thus, an adjuvant treatment that can eliminate tumors with minimizing nerve cell damage would be helpful to minimize the surgical area and to slow down the recurrence of VS.

Here, we demonstrated, by both *in vitro* and *in vivo* experiments, the feasibility of CAP as an adjuvant treatment for eliminating the possible remnant tumor cells in the surgical area after VS excision. The *in vitro* experiments showed that CAP efficiently introduced an anti-proliferative effect on both mouse and human VS cells, by inducing apoptotic, necroptotic, and necrotic cell death. CAP also showed its effectiveness in inducing cell death in patient-derived primary VS cells and tumor mass of 2-mm thickness. In the VS model of SC4-grafted BALB/c nude mouse, CAP treatment after the removal of VS by a microsurgery reduced the size and weight of recurrent tumors. Altogether, these results strongly suggest that CAP should be useful as an adjuvant treatment of VS after surgery to minimize the surgical area and to slow down the recurrence.

In both mouse and human VS cells with *Nf*2 deletion, we showed that CAP treatment induced necrosis as well as apoptotic and necroptotic cell death. Considering that one of the reasons for the failure of chemotherapies in some tumors is a mutation or inhibition of the pathway of cell death [65–68], any anti-tumor therapy that activates different cell death pathways would be a good treatment choice. CAP used in this study would be a promising adjunctive anti-tumor therapy because it causes necrosis even when caspase-dependent apoptosis and RIPK1-RIPK3-dependent necroptosis are blocked.

Recent studies reported that cell death by necroptosis or necrosis may induce an immune response [69], which has its *pros* and *cons*. The immune response would be over-activated by the release of damage-associated molecular patterns (DAMPs) by cell necrosis [70], and the release of these DAMPs may cause severe inflammation [71] and induce endotoxin shock [72]. Conversely, immune cells may be recruited in the area of necroptosis and necrosis and kill the tumor cells that are not directly exposed to CAP [73,74]. Unfortunately, the BALB/c nude mice we used to measure the effect of CAP treatment on VS were immune-deficient and we could not observe the effect of CAP on immune

responses at the surgical areas. We assumed that there might be no detrimental effect of CAP in the physiology of mice since the CAP-treated and -untreated mice showed no difference in lethality. Meanwhile, a potential effect of the CAP therapy on the immune system is still an open question.

VS are benign tumors and only a subset of these tumors develops into malignant tumors as mutations occur in p53 over time [75,76]. Previously, we showed that CAP is more efficient in inducing cell death in p53-deficient cancer cells [22]. CAP has been also reported to delay or prevent the conversion of benign melanocytic tumor to malignant melanoma [77,78]. Thus, if CAP treatment is more effective in p53-mutated VS cells to prevent the conversion to malignancy, it is highly recommendable as an adjunctive therapy for VS after a surgery.

Usually, tumor cells that survived after any anti-proliferative therapy can gain resistance to the therapy applied [59,60]. However, as shown in Fig. 6I and J, CAP-treated VS cells did not become resistant to the cell death induced by subsequent CAP treatment; instead, CAP made the exposed VS cells more vulnerable to cell death by the subsequent treatment partly because CAP induced aneuploidy in the exposed VS cells [61,62]. Thus, when CAP is used as an intra-operative adjuvant therapy for VS, remnant VS cells may become more sensitive even to a subsequent chemotherapy or radiotherapy, if necessary, although these methods have not been efficient in intracranial tumors like VS.

Some studies strongly suggest that a tumor-friendly microenvironment is achieved by local acidification [79,80]. It was observed in several studies that used CAP as an anti-cancer treatment that plasma has increased the acidity in the exposed areas [81,82], presenting a possible drawback of plasma as an anti-cancer therapy. However, CAP generated from the device we designed for *in vivo* treatment did not change the hydrogen ion concentration, as shown in Fig. S1G.

Our air-based CAP devices for *in vivo* and *in vitro* treatment led to apoptotic, necroptotic, and necrotic cell death in human and mouse VS cell lines, and patient-derived primary VS cells. Interestingly, a recent study carried out in mouse 3T3 fibroblast and human mesenchymal stem cells suggested that chemically different non-thermal plasma target distinct cell death pathways [83]. We propose that the cell death pathways activated by CAP treatment may depend not only on the chemical components of the plasma applied, but also on the genetic and physiological background of the cell. Further studies would be needed to correlate the chemical components of plasma to the cell death pathways activated in cells with various genetic and physiological differences.

5. Conclusions

We assessed “the feasibility of cold atmospheric pressure plasma (CAP) as an intra-operative adjuvant treatment modality for vestibular schwannoma after surgery” by investigating the anti-proliferative effect of CAP on human and mouse VS cells, human VS tissues, and VS mouse models after surgery *in vivo*. CAP treatment efficiently induced apoptotic, necroptotic, and necrotic cell death in human VS cells and tissues, without triggering resistance to the subsequent treatment. Our results strongly suggest that CAP should be developed as an efficient adjuvant treatment for VS after surgery to eliminate the possible remnant tumor cells and to minimize the surgical area in the brain for post-surgical wellbeing.

Acknowledgements

None.

Funding

This research was supported by a Grant from the National Research Foundation (NRF) of Korea funded by the Ministry of Science, ICT & Future Planning (Grant number NRF-016M3A9C6918). Yeo Jun Yoon was supported in part by the BK21 and BK21 PLUS program of the NRF of Korea.

Appendix A. Supplementary material

Supplementary data associated with this article can be found in the online version at http://dx.doi.org/10.1016/j.freeradbiomed.2017.11.011.

References

[1] M. Samii, C. Matthies, Management of 1000 vestibular schwannomas (acoustic neuromas): Surgical management and results with an emphasis on complications and how to avoid them, Neurosurgery 40 (1) (1997) 11–21.
[2] M. Sanna, A. Taibah, A. Russo, M. Falcioni, M. Agarwal, Perioperative complications in acoustic neuroma (vestibular schwannoma) surgery, Otol. Neurotol. 25 (3) (2004) 379–386.
[3] J.B. Bederson, K. von Ammon, W.W. Wichmann, G.M. Yasargil, Conservative treatment of patients with acoustic tumors, Neurosurgery 28 (5) (1991) 646–651.
[4] M.E. Glasscock III, D.G. Pappas Jr, S. Manolidis, P.G. Von Doersten, C.G. Jackson, I.S. Storper, Management of acoustic neuroma in the elderly population, Otol. Neurotol. 18 (2) (1997) 236–242.
[5] H.K. El-Kashlan, H. Zeitoun, H.A. Arts, J.T. Hoff, S.A. Telian, Recurrence of acoustic neuroma after incomplete resection, Otol. Neurotol. 21 (3) (2000) 389–392.
[6] H.J. Seol, C.-H. Kim, C.-K. Park, C.H. Kim, D.G. Kim, Y.-S. Chung, H.-W. Jung, Optimal extent of resection in vestibular schwannoma surgery: relationship to recurrence and facial nerve preservation, Neurol. Med.-Chir. 46 (4) (2006) 176–181.
[7] W.Y. Chung, K.D. Liu, C.Y. Shiau, H.M. Wu, L.W. Wang, W.Y. Guo, D.M.T. Ho, D.H.C. Pan, Gamma knife surgery for vestibular schwannoma: 10-year experience of 195 cases, J. Neurosurg. 102 (2005) 87–96.
[8] Y. Iwai, K. Ishibashi, Y. Watanabe, G. Uemura, K. Yamanaka, Functional preservation after planned partial resection followed by gamma knife radiosurgery for large vestibular schwannomas, World Neurosurg. 84 (2) (2015) 292–300.
[9] M.E. Linskey, P.A. Johnstone, M. O'Leary, S. Goetsch, Radiation exposure of normal temporal bone structures during stereotactically guided gamma knife surgery for vestibular schwannomas, J. Neurosurg. 98 (4) (2003) 800–806.
[10] F.C. Timmer, P.E. Hanssens, A.E. van Haren, J.J. Mulder, C.W. Cremers, A.J. Beynon, J.J. van Overbeeke, K. Graamans, Gamma knife radiosurgery for vestibular schwannomas: results of hearing preservation in relation to the cochlear radiation dose, Laryngoscope 119 (6) (2009) 1076–1081.
[11] M. Dobbelstein, U. Moll, Targeting tumour-supportive cellular machineries in anticancer drug development, Nat. Rev. Drug Discov. 13 (3) (2014) 179–196.
[12] A. Wichmann, B. Jaklevic, T.T. Su, Ionizing radiation induces caspase-dependent but Chk2- and p53-independent cell death in Drosophila melanogaster, Proc. Natl. Acad. Sci. USA 103 (26) (2006) 9952–9957.
[13] B. Bucci, S. Misiti, A. Cannizzaro, R. Marchese, G.H. Raza, R. Miceli, A. Stigliano, D. Amendola, O. Monti, M. Biancolella, F. Amati, G. Novelli, A. Vecchione, E. Brunetti, U. De Paula, Fractionated ionizing radiation exposure induces apoptosis through caspase-3 activation and reactive oxygen species generation, Anticancer Res. 26 (6B) (2006) 4549–4557.
[14] I. Tamm, Y. Wang, E. Sausville, D.A. Scudiero, N. Vigna, T. Oltersdorf, J.C. Reed, IAP-family protein survivin inhibits caspase activity and apoptosis induced by Fas (CD95), Bax, caspases, and anticancer drugs, Cancer Res. 58 (23) (1998) 5315–5320.
[15] S. Shin, B.J. Sung, Y.S. Cho, H.J. Kim, N.C. Ha, J.I. Hwang, C.W. Chung, Y.K. Jung, B.H. Oh, An anti-apoptotic protein human survivin is a direct inhibitor of caspase-3 and-7, Biochemistry 40 (4) (2001) 1117–1123.
[16] M. Hassounah, B. Lach, A. Allam, H. Al-Khalaf, Y. Siddiqui, N. Pangue-Cruz, A. Al-Omeir, M.N. Al-Ahdal, A. Aboussekhra, Benign tumors from the human nervous system express high levels of survivin and are resistant to spontaneous and radiation-induced apoptosis, J. Neurooncol. 72 (3) (2005) 203–208.
[17] S. Ammoun, C.O. Hanemann, Emerging therapeutic targets in schwannomas and other merlin-deficient tumors, Nat. Rev. Neurol. 7 (7) (2011) 392–399.
[18] C.O. Hanemann, D.G. Evans, News on the genetics, epidemiology, medical care and translational research of Schwannomas, J. Neurol. 253 (12) (2006) 1533–1541.
[19] G. Fridman, G. Friedman, A. Gutsol, A.B. Shekhter, V.N. Vasilets, A. Fridman, Applied plasma medicine, Plasma Process. Polym. 5 (6) (2008) 503–533.
[20] K. Song, G. Li, Y. Ma, A review on the selective apoptotic effect of nonthermal atmospheric-pressure plasma on cancer cells, 4(1–4), 2014, pp. 193–209.
[21] A. Siu, O. Volotskova, X.Q. Cheng, S.S. Khalsa, K. Bian, F. Murad, M. Keidar, J.H. Sherman, Differential effects of cold atmospheric plasma in the treatment of malignant glioma, PLoS One 10 (6) (2015).
[22] Y.H. Ma, C.S. Ha, S.W. Hwang, H.J. Lee, G.C. Kim, K.W. Lee, K. Song, Non-thermal atmospheric pressure plasma preferentially induces apoptosis in p53-mutated cancer cells by activating ROS stress-response pathways, PLoS One 9 (4) (2014).
[23] M. Ishaq, S. Kumar, H. Varinli, Z.J. Han, A.E. Rider, M.D.M. Evans, A.B. Murphy, K. Ostrikov, Atmospheric gas plasma-induced ROS production activates TNF-ASK1 pathway for the induction of melanoma cancer cell apoptosis, Mol. Biol. Cell 25 (9) (2014) 1523–1531.
[24] X.Q. Cheng, J. Sherman, W. Murphy, E. Ratovitski, J. Canady, M. Keidar, The effect of tuning cold plasma composition on glioblastoma cell viability, PLoS One 9 (5)

(2014).
[25] B. Gweon, M. Kim, D.B. Kim, D. Kim, H. Kim, H. Jung, J.H. Shin, W. Choe, Differential responses of human liver cancer and normal cells to atmospheric pressure plasma, Appl. Phys. Lett. 99 (6) (2011).
[26] B.S. Kwon, E.H. Choi, B. Chang, J.H. Choi, K.S. Kim, H.K. Park, Selective cytotoxic effect of non-thermal micro-DBD plasma, Phys. Biol. 13 (5) (2016) 056001.
[27] S.H. Ji, K.H. Choi, A. Pengkit, J.S. Im, J.S. Kim, Y.H. Kim, Y. Park, E.J. Hong, S.K. Jung, E.H. Choi, G. Park, Effects of high voltage nanosecond pulsed plasma and micro DBD plasma on seed germination, growth development and physiological activities in spinach, Arch. Biochem. Biophys. 605 (2016) 117–128.
[28] Y.J. Yoon, G. Li, G.C. Kim, H.J. Lee, K. Song, Effects of 60-Hz time-varying electric fields on DNA damage and cell viability support negligible genotoxicity of the electric fields, J. Electromagn. Eng. Sci. 15 (3) (2015) 134–141.
[29] N. Kurake, H. Tanaka, K. Ishikawa, T. Kondo, M. Sekine, K. Nakamura, H. Kajiyama, F. Kikkawa, M. Mizuno, M. Hori, Cell survival of glioblastoma grown in medium containing hydrogen peroxide and/or nitrite, or in plasma-activated medium, Arch. Biochem. Biophys. 605 (2016) 102–108.
[30] H. Morrison, T. Sperka, J. Manent, M. Giovannini, H. Ponta, P. Herrlich, Merlin/neurofibromatosis type 2 suppresses growth by inhibiting the activation of Ras and Rac, Cancer Res. 67 (2) (2007) 520–527.
[31] J.T. Fraenzer, H. Pan, L. Minimo Jr., G.M. Smith, D. Knauer, G. Hung, Overexpression of the NF2 gene inhibits schwannoma cell proliferation through promoting PDGFR degradation, Int. J. Oncol. 23 (6) (2003) 1493–1500.
[32] H. Lecoeur, Nuclear apoptosis detection by flow cytometry: influence of endogenous endonucleases, Exp. Cell Res. 277 (1) (2002) 1–14.
[33] Y. Pan, A. Leifert, D. Ruau, S. Neuss, J. Bornemann, G. Schmid, W. Brandau, U. Simon, W. Jahnen-Dechent, Gold nanoparticles of diameter 1.4 nm trigger necrosis by oxidative stress and mitochondrial damage, Small 5 (18) (2009) 2067–2076.
[34] N. Kaushik, N. Uddin, G.B. Sim, Y.J. Hong, K.Y. Baik, C.H. Kim, S.J. Lee, N.K. Kaushik, E.H. Choi, Responses of solid tumor cells in DMEM to reactive oxygen species generated by non-thermal plasma and chemically induced ROS systems, Sci. Rep.-Uk 5 (2015).
[35] L.K. Chin, J.Q. Yu, Y. Fu, T. Yu, A.Q. Liu, K.Q. Luo, Production of reactive oxygen species in endothelial cells under different pulsatile shear stresses and glucose concentrations, Lab Chip 11 (11) (2011) 1856–1863.
[36] S. Bekeschus, J. Kolata, C. Winterbourn, A. Kramer, R. Turner, K.D. Weltmann, B. Broker, K. Masur, Hydrogen peroxide: a central player in physical plasma-induced oxidative stress in human blood cells, Free Radic. Res. 48 (5) (2014) 542–549.
[37] V. Vallyathan, V. Castranova, X. Shi, Oxygen/Nitrogen Radicals: Cell Injury and Disease, 'Redox Signaling' by H.J. Forman, M. Torres and J. Fukuto, Springer Science & Business Media, 2002, pp.58–59.
[38] I. Vermes, C. Haanen, H. Steffens-Nakken, C. Reutelingsperger, A novel assay for apoptosis. Flow cytometric detection of phosphatidylserine expression on early apoptotic cells using fluorescein labelled Annexin V, J. Immunol. Methods 184 (1) (1995) 39–51.
[39] I. Schmid, C.H. Uittenbogaart, B. Keld, J.V. Giorgi, A rapid method for measuring apoptosis and dual-color immunofluorescence by single laser flow cytometry, J. Immunol. Methods 170 (2) (1994) 145–157.
[40] D. Vercammen, R. Beyaert, G. Denecker, V. Goossens, G. Van Loo, W. Declercq, J. Grooten, W. Fiers, P. Vandenabeele, Inhibition of caspases increases the sensitivity of L929 cells to necrosis mediated by tumor necrosis factor, J. Exp. Med. 187 (9) (1998) 1477–1485.
[41] K. Schulzeosthoff, A.C. Bakker, B. Vanhaesebroeck, R. Beyaert, W.A. Jacob, W. Fiers, Cytotoxic activity of tumor-necrosis-factor Is mediated by early damage of mitochondrial functions - evidence for the involvement of mitochondrial radical generation, J. Biol. Chem. 267 (8) (1992) 5317–5323.
[42] T. Vanden Berghe, N. Vanlangenakker, E. Parthoens, W. Deckers, M. Devos, N. Festjens, C.J. Guerin, U.T. Brunk, W. Declercq, P. Vandenabeele, Necroptosis, necrosis and secondary necrosis converge on similar cellular disintegration features, Cell Death Differ. 17 (6) (2010) 922–930.
[43] T. Vanden Berghe, A. Linkermann, S. Jouan-Lanhouet, H. Walczak, P. Vandenabeele, Regulated necrosis: the expanding network of non-apoptotic cell death pathways, Nat. Rev. Mol. Cell Biol. 15 (2) (2014) 135–147.
[44] S.W. Yu, H. Wang, M.F. Poitras, C. Coombs, W.J. Bowers, H.J. Federoff, G.G. Poirier, T.M. Dawson, V.L. Dawson, Mediation of poly(ADP-ribose) polymerase-1-dependent cell death by apoptosis-inducing factor, Science 297 (5579) (2002) 259–263.
[45] C. Fiorillo, V. Ponziani, L. Giannini, C. Cecchi, A. Celli, N. Nassi, L. Lanzilao, R. Caporale, P. Nassi, Protective effects of the PARP-1 inhibitor PJ34 in hypoxic-reoxygenated cardiomyoblasts, Cell Mol. Life Sci. 63 (24) (2006) 3061–3071.
[46] H. Wang, L. Sun, L. Su, J. Rizo, L. Liu, L.F. Wang, F.S. Wang, X. Wang, Mixed lineage kinase domain-like protein MLKL causes necrotic membrane disruption upon phosphorylation by RIP3, Mol. Cell 54 (1) (2014) 133–146.
[47] L.J. Su, B. Quade, H.Y. Wang, L.M. Sun, X.D. Wang, J. Rizo, A plug release mechanism for membrane permeation by MLKL, Structure 22 (10) (2014) 1489–1500.
[48] M.J. Morgan, Y.S. Kim, The serine threonine kinase RIP3: lost and found, BMB Rep. 48 (6) (2015) 303–312.
[49] Q. Remijsen, V. Goossens, S. Grootjans, C. Van den Haute, N. Vanlangenakker, Y. Dondelinger, R. Roelandt, I. Bruggeman, A. Goncalves, M.J. Bertrand, V. Baekelandt, N. Takahashi, T.V. Berghe, P. Vandenabeele, Depletion of RIPK3 or MLKL blocks TNF-driven necroptosis and switches towards a delayed RIPK1 kinase-dependent apoptosis, Cell Death Dis. 5 (2014) e1004.
[50] M. Garcia-Calvo, E.P. Peterson, B. Leiting, R. Ruel, D.W. Nicholson, N.A. Thornberry, Inhibition of human caspases by peptide-based and macromolecular inhibitors, J. Biol. Chem. 273 (49) (1998) 32608–32613.
[51] A. Degterev, J. Hitomi, M. Germscheid, I.L. Ch'en, O. Korkina, X. Teng, D. Abbott, G.D. Cuny, C. Yuan, G. Wagner, S.M. Hedrick, S.A. Gerber, A. Lugovskoy, J. Yuan, Identification of RIP1 kinase as a specific cellular target of necrostatins, Nat. Chem. Biol. 4 (5) (2008) 313–321.
[52] Z. Ma, Q. Wei, G. Dong, Y. Huo, Z. Dong, DNA damage response in renal ischemia-reperfusion and ATP-depletion injury of renal tubular cells, Biochim. Biophys. Acta 1842 (7) (2014) 1088–1096.
[53] Z.J. Zhou, B. Lu, C. Wang, Z.Q. Wang, T.F. Luo, M.H. Piao, F.K. Meng, G.F. Chi, Y.N. Luo, P.F. Ge, RIP1 and RIP3 contribute to shikonin-induced DNA double-strand breaks in glioma cells via increase of intracellular reactive oxygen species, Cancer Lett. 390 (2017) 77–90.
[54] V. Marx, Cell-line authentication demystified, Nat. Methods 11 (5) (2014) 483–488.
[55] H. Jablonowski, T. von Woedtke, Research on plasma medicine-relevant plasma--liquid interaction: what happened in the past five years? Clin. Plasma Med. 3 (2) (2015) 42–52.
[56] E.J. Szili, J.W. Bradley, R.D. Short, A 'tissue model' to study the plasma delivery of reactive oxygen species, J. Phys. D Appl. Phys. 47 (15) (2014).
[57] M. Ishaq, A. Rowe, K. Bazaka, M. Krockenberger, M.D.M. Evans, K. Ostrikov, Effect of atmospheric-pressure plasmas on drug resistant melanoma: the challenges of translating in vitro outcomes into animal models, Plasma Med. 6 (1) (2016) 67–83.
[58] H. Tanaka, M. Mizuno, K. Ishikawa, K. Nakamura, H. Kajiyama, H. Kano, F. Kikkawa, M. Hori, Plasma-activated medium selectively kills glioblastoma brain tumor cells by down-regulating a survival signaling molecule, AKT Kinase 1 (3–4) (2011) 265–277.
[59] G.L. Beretta, L. Gatti, P. Perego, N. Zaffaroni, Camptothecin resistance in cancer: insights into the molecular mechanisms of a DNA-damaging drug, Curr. Med. Chem. 20 (12) (2013) 1541–1565.
[60] H. Zahreddine, K.L.B. Borden, Mechanisms and insights into drug resistance in cancer, Front. Pharmacol. 4 (2013).
[61] G.R. Gorla, H. Malhi, S. Gupta, Polyploidy associated with oxidative injury attenuates proliferative potential of cells, J. Cell Sci. 114 (16) (2001) 2943–2951.
[62] S. Gupta, Hepatic polyploidy and liver growth control, Semin Cancer Biol. 10 (3) (2000) 161–171.
[63] O. Bloch, M.E. Sughrue, R. Kaur, A.J. Kane, M.J. Rutkowski, G. Kaur, I. Yang, L.H. Pitts, A.T. Parsa, Factors associated with preservation of facial nerve function after surgical resection of vestibular schwannoma, J. Neuro-Oncol. 102 (2) (2011) 281–286.
[64] J.G. Rowe, M.W. Radatz, L. Walton, T. Soanes, J. Rodgers, A.A. Kemeny, Clinical experience with gamma knife stereotactic radiosurgery in the management of vestibular schwannomas secondary to type 2 neurofibromatosis, J. Neurol. Neurosurg. Psychiatry 74 (9) (2003) 1288–1293.
[65] D. Hanahan, R.A. Weinberg, Hallmarks of cancer: the next generation, Cell 144 (5) (2011) 646–674.
[66] R. Gerl, D.L. Vaux, Apoptosis in the development and treatment of cancer, Carcinogenesis 26 (2) (2005) 263–270.
[67] J.M. Brown, L.D. Attardi, Opinion - the role of apoptosis in cancer development and treatment response, Nat. Rev. Cancer 5 (3) (2005) 231–237.
[68] D. Hanahan, R.A. Weinberg, The hallmarks of cancer, Cell 100 (1) (2000) 57–70.
[69] S.Y. Seong, P. Matzinger, Hydrophobicity: an ancient damage-associated molecular pattern that initiates innate immune responses, Nat. Rev. Immunol. 4 (6) (2004) 469–478.
[70] A.M. Farkas, T.M. Kilgore, M.T. Lotze, Editorial overview detecting DNA: getting and begetting cancer, Curr. Opin. Invest Dr 8 (12) (2007) 981–986.
[71] P. Scaffidi, T. Misteli, M.E. Bianchi, Release of chromatin protein HMGB1 by necrotic cells triggers inflammation, Nature 418 (6894) (2002) 191–195.
[72] H.C. Wang, O. Bloom, M.H. Zhang, J.M. Vishnubhakat, M. Ombrellino, J.T. Che, A. Frazier, H. Yang, S. Ivanova, L. Borovikova, K.R. Manogue, E. Faist, E. Abraham, J. Andersson, U. Andersson, P.E. Molina, N.N. Abumrad, A. Sama, K.J. Tracey, HMG-1 as a late mediator of endotoxin lethality in mice, Science 285 (5425) (1999) 248–251.
[73] D.V. Krysko, A.D. Garg, A. Kaczmarek, O. Krysko, P. Agostinis, P. Vandenabeele, Immunogenic cell death and DAMPs in cancer therapy, Nat. Rev. Cancer 12 (12) (2012) 860–875.
[74] R. Spisek, M.V. Dhodapkar, Towards a better way to die with chemotherapy - role of heat shock protein exposure on dying tumor cells, Cell Cycle 6 (16) (2007) 1962–1965.
[75] A.H.P.P. Dayalan, M. Jothi, R. Keshava, R. Thomas, M.L. Gope, S.K. Doddaballapur, S. Somanna, S.S. Praharaj, C.B. Ashwathnarayanarao, R. Gope, Age dependent phosphorylation and deregulation of p53 in human vestibular Schwannomas, Mol. Carcinog. 45 (1) (2006) 38–46.
[76] E. Robanus-Maandag, M. Giovannini, M. van der Valk, M. Niwa-Kawakita, V. Abramowski, C. Antonescu, G. Thomas, A. Berns, Synergy of Nf2 and p53 mutations in development of malignant tumours of neural crest origin, Oncogene 23 (39) (2004) 6541–6547.
[77] Y. Omata, M. Iida, I. Yajima, K. Takeda, N. Ohgami, M. Hori, M. Kato, Non-thermal atmospheric pressure plasmas as a novel candidate for preventive therapy of melanoma, Environ. Health Prev. Med. 19 (5) (2014) 367–369.
[78] Y. Omata, M. Iida, I. Yajima, N. Ohgami, M. Maeda, H. Ninomiya, R. Oshino, T. Tsuzuki, M. Hori, M. Kato, Modulated expression levels of tyrosine kinases in spontaneously developed melanoma by single irradiation of non-thermal atmospheric pressure plasmas, Int. J. Clin. Exp. Patho 9 (2) (2016) 1061–1067.
[79] V. Estrella, T. Chen, M. Lloyd, J. Wojtkowiak, H.H. Cornnell, A. Ibrahim-Hashim, K. Bailey, Y. Balagurunathan, J.M. Rothberg, B.F. Sloane, J. Johnson, R.A. Gatenby, R.J. Gillies, Acidity generated by the tumor microenvironment drives local invasion, Cancer Res. 73 (5) (2013) 1524–1535.

[80] Y. Kato, S. Ozawa, C. Miyamoto, Y. Maehata, A. Suzuki, T. Maeda, Y. Baba, Acidic extracellular microenvironment and cancer, Cancer Cell Int. 13 (2013).
[81] J. Balzer, K. Heuer, E. Demir, M.A. Hoffmanns, S. Baldus, P.C. Fuchs, P. Awakowicz, C.V. Suschek, C. Oplander, Non-thermal Dielectric Barrier Discharge (DBD) effects on proliferation and differentiation of human fibroblasts are primary mediated by hydrogen peroxide, PLoS One 10 (12) (2015) e0144968.
[82] M. Vandamme, E. Robert, S. Pesnel, E. Barbosa, S. Dozias, J. Sobilo, S. Lerondel, A. Le Pape, J.M. Pouvesle, Antitumor effect of plasma treatment on U87 glioma xenografts: preliminary results, Plasma Process. Polym. 7 (3–4) (2010) 264–273.
[83] O. Lunov, V. Zablotskii, O. Churpita, M. Lunova, M. Jirsa, A. Dejneka, S. Kubinova, Chemically different non-thermal plasmas target distinct cell death pathways, Sci. Rep.-Uk 7 (2017).